Fractionalization Waves in Two-Dimensional Dirac Fermions: Quantum Imprint from One Dimension

Seth M. Davis[1] and Matthew S. Foster[1,2]
[1]Department of Physics and Astronomy, Rice University, Houston, Texas 77005, USA
[2]Rice Center for Quantum Materials, Rice University, Houston, Texas 77005, USA

(Received 14 September 2018; published 14 February 2019)

Particle fractionalization is believed to orchestrate the physics of many strongly correlated systems, yet its direct experimental detection remains a challenge. We propose a simple measurement for an ultracold matter system, in which correlations in initially decoupled 1D chains are imprinted via quantum quench upon two-dimensional Dirac fermions. Luttinger liquid correlations launch relativistic "fractionalization waves" along the chains, while coupling noninteracting chains induces perpendicular dispersion. These could be easily distinguished in an ultracold gas experiment.

DOI: 10.1103/PhysRevLett.122.065302

Fractionalization is a profound, nonperturbative effect of interparticle interactions in quantum matter, in which the emergent degrees of freedom (d.o.f.) of a strongly correlated system can be neither bosonic nor fermionic. Fractionalization may reside at the heart of high-temperature superconductivity and spin liquid physics [1,2]. Although an essential characteristic of the fractional quantum Hall effect (FQHE) that may enable topological quantum computation [3], the direct detection of fractionalization in solid state experiments has proven to be challenging [4].

In this Letter, we propose an ultracold fermion gas experiment that could detect a clear signal for fractionalization, using currently available experimental techniques. In comparison to the much more daunting task of realizing a FQHE state of interacting fermions in cold atoms [5], we require only the preparation of 1D fermionic Luttinger liquids (as recently measured in Refs. [6,7]), that can be coupled together via a quantum quench [8] into a 2D pi-flux lattice (as recently realized in Refs. [9–11]). We predict discriminating signatures in density waves launched from an initial Gaussian bump at the time of the quench. Any degree of fractionalization produces waves with a characteristic shape profile that propagate at the "speed of light" along the 1D chains. By contrast, a noninteracting prequench system induces simple dispersion perpendicular to the chains.

Fractionalization can arise in a many-fermion system when the fermion operator acquires an anomalous dimension, due to interactions [12,13]. In our proposed experiment, a nonzero fermion anomalous dimension directly determines density wave dynamics in a two-dimensional (2D) fermion system. Here Luttinger liquid correlations [14,15] in a system of initially decoupled 1D chains are *imprinted* upon two-dimensional Dirac fermions. This is accomplished via a quantum quench [16–25] that couples together the chains into a 2D pi-flux lattice model (see Fig. 1). To probe the dynamics, we calculate the density waves emitted from an initial density bump [26–36]. We show that a nonzero initial-state-fermion anomalous dimension launches relativistic "fractionalization waves" along the chains, shown in Fig. 2. By contrast, the same quench performed from initially noninteracting chains induces dispersive propagation perpendicular to the chains, see Fig. 3. The key result of this work is that the orthogonal

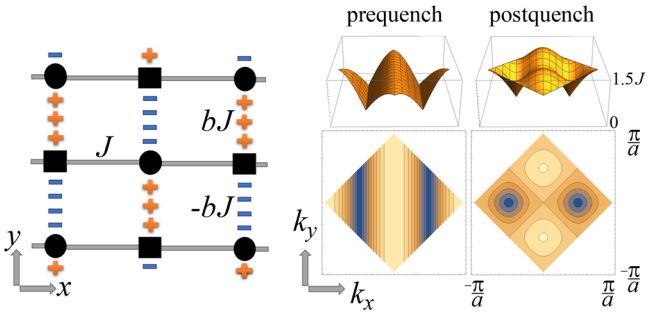

FIG. 1. Lattice setup for quench-induced fractionalization waves. We consider fermions hopping on a pi-flux square lattice (left), with horizontal bonds of strength J and sign-staggered vertical bonds of strength bJ. The Hamiltonian for the noninteracting model is given by Eq. (1). We quench from the decoupled chain limit ($b = 0$) to $b > 0$. We assume that interactions can induce Luttinger liquid correlations (charge fractionalization) along the chains in the prequench state. The latter are imprinted by the quench upon the pi-flux band fermions, leading to the two-dimensional density wave dynamics depicted in Fig. 2 (fractionalized) and Fig. 3 (not fractionalized, initially noninteracting). The right panels in this figure show the pre- and postquench energy bands. The prequench state of decoupled chains is characterized by vertical nodal lines. The postquench band gaps these out, except for a pair of Dirac points at $\{k_x, k_y\} = \{\pm\pi/2a, 0\}$. Energy bands are depicted over the reduced Brillouin zone of the pi-flux lattice; a denotes the lattice constant.

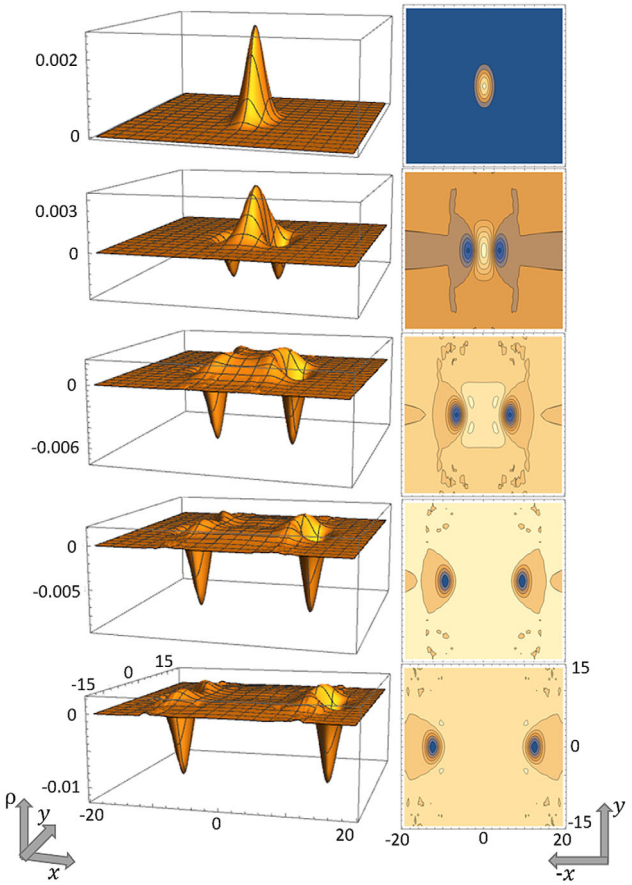

FIG. 2. Quench from decoupled chains to the pi-flux lattice I: horizontal, "relativistic" fractionalization waves. A positive Gaussian density bump is superimposed by an external potential on top of decoupled Luttinger liquids in the initial state. Via instantaneous quench, the interchain coupling is turned on, while the bump is released by turning off the potential. In this figure we plot the time evolution of the post-quench density profile $\rho(t, x, y)$, assuming charge fractionalization of the initial Luttinger liquid. Left (right) panels show the density in profile (contour) plots; *negative* density means a depletion of the filled Fermi sea. Total particle number is conserved [37]. The above plots give time-slice profiles at $t = 0$, 3, 6, 9, 12 (where t is in units of v_F/a). The degree of fractionalization is characterized by the fermion anomalous dimension $\eta = 0.7$ [Eq. (5)]. We also incorporate a small but positive initial Fermi momentum, $k_F = 0.1/a$. The other initial configuration parameters are $\{Q = 0.1, \Delta_x = 2a, \Delta_y = 3a\}$ [Eq. (6)], and we time evolve with the Hamiltonian parameters $\{v_F = b = 1\}$. We choose a small bump to conserve computational resources, but in an experiment a larger bump would minimize lattice-scale detail neglected in Eq. (5) [37].

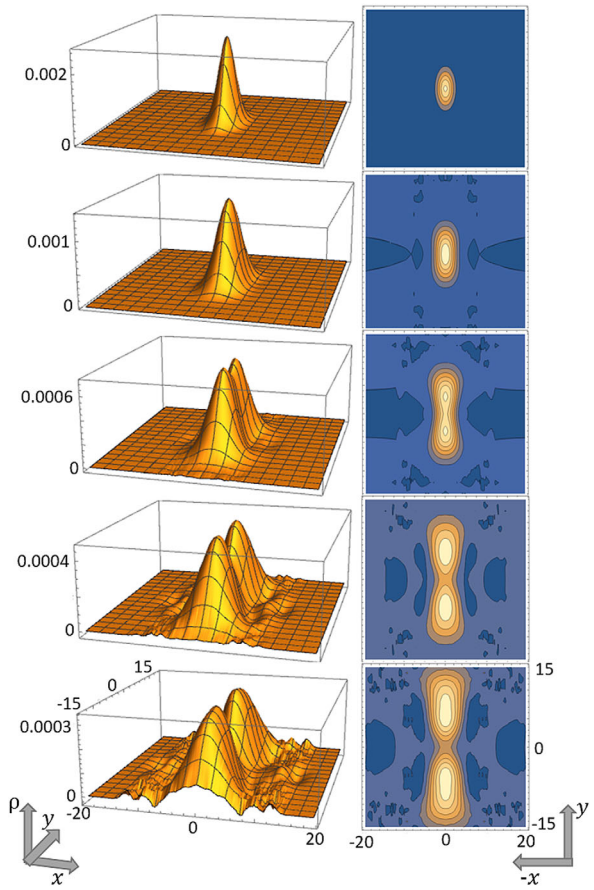

FIG. 3. Quench from decoupled chains to the pi-flux lattice II: dispersing vertical density waves from nonfractionalized (noninteracting) chains. The absence of relativistic propagation in the horizontal direction is due to Pauli blocking (see text and Fig. 4). We plot the same time evolution of the post-quench density profile as in Fig. 2, but for a vanishing prequench fermion anomalous dimension $\eta = 0$. All other parameters are identical to Fig. 2. The plots show profiles at $t = 0$, 3, 6, 9, 12.

motions of the fractionalized and noninteracting cases should be easily distinguishable in an ultracold fermion experiment.

Similar fractionalization waves dubbed "supersolitons" were previously predicted in 1D quenches, including the continuum sine-Gordon model [27] and the XXZ chain [28]. As in those studies, correlations shape the initial condition, but we ignore interactions in the postquench evolution. In an ultracold fermion gas it might be possible to turn off the interactions at the time of the quench, but this is not a requirement for us. Interactions are strongly irrelevant (in the sense of the renormalization group) in the postquench band structure. Our results should hold over a tunable transient window $0 \le t < \tau_{\mathrm{col}}$, where $1/\tau_{\mathrm{col}}$ is the particle-particle scattering rate determined by the interactions and the postquench energy density.

Model.—We consider a pi-flux lattice model for fermions in two dimensions,

$$H = -J\sum_{m,n} c^{\dagger}_{m,n}[c_{m+1,n} + b(-1)^{m+n}c_{m,n+1}] + \mathrm{H.c.}, \qquad (1)$$

where $c_{m,n}$ annihilates a fermion at site $\{x, y\} = \{m, n\}a$ of the square lattice, a is the lattice spacing, and $J > 0$ is the hopping energy. The dimensionless anisotropy parameter b controls the strength of the staggered vertical hopping

(see Fig. 1). We work with spinless fermions without loss of generality. Spin-1/2 particles would be advantageous in an ultracold fermion experiment, as decoupled Hubbard chains in the prequench state give a particular way to realize tunable charge fractionalization via the on-site Hubbard U interaction (at densities away from half-filling) [15]. Apart from this, physical spin will not impact the dynamics discussed here.

The system is assumed to initially have $b = 0$, so that the lattice reduces to a set of uncoupled 1D chains. The noninteracting band structure consists of vertical nodal lines. Via instantaneous quantum quench, b is switched to a positive, nonzero value, gapping out the nodal lines except for a pair of Dirac points at $\{k_x, k_y\} = \{\pm\pi/2a, 0\}$. The pi flux ensures that the low-energy sectors of the pre- and postquench band structures overlap.

We assume that the main effect of the global quench is to excite particle-hole pairs along the nodal lines of the prequench band structure. We therefore retain momentum modes along narrow channels including these, $\{|k_x \pm \pi/2a| \leq \Lambda, |k_y| \leq \pi/2a\}$. Here $\Lambda \ll \pi/a$ is a momentum cutoff. Eq. (1) can then be approximated as

$$H \simeq v_F \int_{-\Lambda}^{\Lambda} \frac{dk_x}{2\pi} \int_{-\frac{\pi}{2a}}^{\frac{\pi}{2a}} \frac{dk_y}{2\pi} \psi^\dagger(\mathbf{k}) \hat{h}(\mathbf{k}) \psi(\mathbf{k}) + \int dx dy \psi^\dagger(x,y) \psi(x,y) \Phi(x,y) + H_I, \quad (2a)$$

$$\hat{h}(\mathbf{k}) \equiv \hat{\sigma}^3 k_x + \hat{\sigma}^2 m(k_y), \quad (2b)$$

where $v_F = 2Ja$ is the maximum band velocity. The field $\psi(\mathbf{k}) \to \psi_{\sigma,\tau}(\mathbf{k})$ is a four-component spinor. The Pauli matrices $\hat{\sigma}^{1,2,3}$ act on the space of right ($\sigma^3 = 1$) and left ($\sigma^3 = -1$) movers in the initial decoupled chains; this is *not* equivalent to the space of right and left nodal lines (see Ref. [37] for details). Equation (2a) is invariant under SU(2) rotations on the index $\tau \in \{1, 2\}$, which distinguishes modes whose k_y momenta fall in or outside the *reduced* Brillouin zone (RBZ) depicted in Fig. 1. The parameter

$$m(k_y) \equiv (b/a) \sin(k_y a) \quad (3)$$

in Eq. (2b) plays the role of a k_y-dependent "mass," when the system is viewed as a collection of decoupled 1D chains. Linearizing near $k_y = 0$ with $b = 1$ would give isotropic massless 2D Dirac fermions.

Relative to the homogeneous, noninteracting lattice model in Eq. (1), we have incorporated two additional perturbations on the second line of Eq. (2a). The first is an inhomogeneous external potential $\Phi(x, y)$. We assume a localized potential profile in the prequench state. Via the axial anomaly, this induces an initial density inhomogeneity in the decoupled chains of the form $\rho(x, y) = -\kappa\Phi(x, y)$, where κ is the compressibility. After the quench we will set $\Phi = 0$, and we will monitor the evolution of $\rho(t, x, y)$ as a probe of the dynamics.

Although Eq. (1) with $b = 0$ describes decoupled chains for spinless fermions, the field $\psi_{\sigma,\tau}$ consists of four, not two components. The synthetic τ-spin d.o.f. is an artifact of folding into the RBZ, necessary for describing the pi-flux lattice. The term H_I in Eq. (2a) encodes generic short-ranged intrachain fermion-fermion interactions. It is well known that the low-energy theory for a single-channel, spin-1/2 SU(2)-symmetric quantum wire (described via a four-component field ψ) admits four independent local, four-fermion interaction operators [15]. This includes spin current-current and charge umklapp interactions, and these can gap out the spin or charge d.o.f. In our case the coupling constants of these operators should be tuned precisely to zero, because these describe interactions between *pairs* of chains. The admissible interactions [charge current-current and U(1) stress tensor operators] set the charge velocity and Luttinger parameter K in the prequench Luttinger liquid state of the decoupled chains [37].

At time $t = 0$, we quench on the interchain coupling $b > 0$, and turn off the potential Φ and interactions in H_I. (In fact, we argue later that interactions can remain in place, and will produce a negligible effect on the dynamics up to time τ_{col}, defined below). Then the time-evolving density profile is determined by the convolution

$$\rho(t, x, y) = \int dx_1\, dx_2\, dy_1 \mathrm{Tr}[\hat{G}^\dagger(t, x_1, y_1) \hat{G}(t, x_2, y_1)] \times \mathcal{C}_\Phi(x - x_1, x - x_2; y - y_1), \quad (4)$$

where $\hat{G}(t, x_1, y_1)$ is the causal Green's function associated to $\hat{h}$, and $\mathcal{C}_\Phi(x_1, x_2; y)$ describes the static one-particle fermion correlation function in the initial state at linear order in the external potential Φ, given by [28,37]

$$\mathcal{C}_\Phi(x_1, x_2; y) = \frac{c_\eta}{2} \left(\frac{\alpha^2}{(x_{12})^2 + \zeta^2} \right)^{\eta/2} \frac{\int_{x_1}^{x_2} dx\, \kappa\Phi(x, y)}{x_{12}}, \quad (5)$$

where $x_{12} = x_1 - x_2$. Here c_η and α are positive constants, while η is the fermion anomalous dimension. The latter is $\eta = (1/2^p)(K + K^{-1} - 2)$, where K is the Luttinger parameter [14,15]. The exponent $p = 1$ ($p = 2$) for spinless (spin-1/2) fermions within each chain. $K = 1$ gives $\eta = 0$ (noninteracting chains); otherwise $\eta > 0$. The parameter ζ is a short-distance regularization that can affect the dynamics at long times [28]. Equation (5) is appropriate for half-filling ($k_F = 0$). We compare the results from this correlator with an exact lattice quench in the free fermion case in Ref. [37].

Results.—We numerically integrate Eq. (4), using Eq. (5) and assuming a Gaussian potential

$$\kappa\Phi(x, y) = Q(\pi\Delta_x\Delta_y)^{-1} e^{-(x/\Delta_x)^2 - (y/\Delta_y)^2}. \quad (6)$$

We set the parameter $\alpha = a = 1$ in Eq. (5) [37].

As is clear from Figs. 2 and 3, the qualitative behavior of the postquench density profile depends crucially on whether or not the initial state is fractionalized. In the initially fractionalized case [$\eta > 0$ in Eq. (5), Fig. 2], the density develops collective excitations that propagate horizontally along the chains at the maximum band velocity v_F. These fractionalization waves ("supersolitons" [27,28]) retain their shape as they travel and exhibit power-law growth of amplitude with time. Supersolitons possess positive peaks and negative-density troughs; the total particle number induced by the initial potential on top of the filled Fermi sea is preserved at all times [37]. The results in Fig. 2 obtain from Eq. (5) with no short-distance regularization, $\zeta = 0$. Nonzero ζ can arise due to the effects of irrelevant operators [28], but we show in Ref. [37] that qualitatively identical dynamics obtain in this case except at long times, wherein the supersoliton growth is curtailed [28]. By contrast, for the noninteracting initial condition ($\eta = 0$, Fig. 3), there is no supersoliton and the initial density disperses vertically, perpendicular to the chains.

The density dynamics in Figs. 2 and 3 should be contrasted with one-particle quantum mechanics. The same Green's function $\hat{G}(t, x, y)$ that enters into Eq. (4) determines the evolution of a Gaussian single-particle wave packet. Since $\hat{h} \simeq -i\hat{\sigma}^3\partial_x - i\hat{\sigma}^2\partial_y$, the result is a circular wave front propagating at the "speed of light" [37]. Instead, the fractionalized quench gives x-directed supersolitons, while the noninteracting quench gives y-dispersing propagation. The difference between the latter and one-particle quantum mechanics is due to Pauli blocking [28]. Single-particle quantum mechanics also shows that lattice-scale detail neglected in the Green's function has negligible effect on the dynamics over the timescales of interest [37].

Further insight into the quench dynamics obtains from the Wigner distribution due to the initial Gaussian bump,

$$\delta n_+(v_x, v_y; R_x, R_y) \propto \mathcal{J}(\boldsymbol{v}) \int d^2\mathbf{q} e^{i\mathbf{q}\cdot\mathbf{R}} \times \langle a^\dagger[\mathbf{k}(\boldsymbol{v}) - \mathbf{q}/2] a[\mathbf{k}(\boldsymbol{v}) + \mathbf{q}/2]\rangle_\Phi, \tag{7}$$

where $a(\mathbf{k})$ annihilates a pi-flux conduction band fermion with momentum $\mathbf{k}$, and $\mathcal{J}(\boldsymbol{v}) \equiv |\partial k_\mu / \partial v_\nu|$ is the Jacobian relating the postquench band velocities $v_{x,y} \equiv \partial_{k_{x,y}} \sqrt{k_x^2 + m^2(k_y)}$ to the momenta $k_{x,y}$. The expectation value in Eq. (7) is computed at time $t = 0$, i.e., using Eq. (5). The Wigner distribution is plotted for variable η in Fig. 4. We observe a pronounced difference between the fractionalized and nonfractionalized cases. The distribution for the case with $\eta > 0$ has a diverging density of x-direction velocities approaching the maximum band velocity. On the other hand, the noninteracting $\eta = 0$ case has a velocity distribution strongly localized to x velocities close to zero. The absence of large x velocities in the latter is due to Pauli blocking: for $k_y = 0$, the momentum $|q_x|$ must exceed $2|k_x|$ in order for the pair of operators in Eq. (7) to create a particle-hole pair in the Fermi sea. Large $|q_x| > 1/\Delta_x$ (and therefore large v_x) is suppressed by the initial density profile [Eq. (6)]. Fractionalization ($\eta > 0$) circumnavigates the Pauli blocking restriction on large x velocities [37]. This is because the fermions responsible for the postquench propagation are not locally related to the effectively noninteracting, but fractionally charged constituents that define the prequench vacuum state [28]. We also note that the kinematic condition

$$v_x^2 + v_y^2/b^2 \leq 1, \tag{8}$$

implies that the accumulation of the Wigner distribution at $v_x = 1$ requires $v_y = 0$, and thus explains why the supersoliton is stable to dispersion in the y direction.

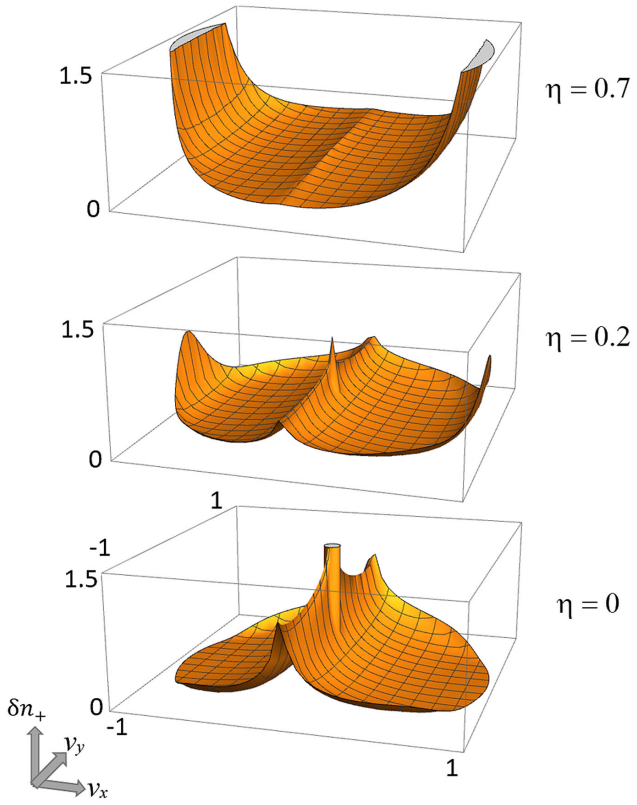

FIG. 4. Wigner velocity distribution $\delta n_+(v_x, v_y; R_x, R_y)$ imprinted on the pi-flux band fermions at the time of the quench, induced by charge fractionalization and a Gaussian density bump in the initial state of decoupled chains. The distribution is evaluated at the center of the bump $R_x = R_y = 0$. Unlike continuum 2D massless Dirac fermions, the allowed velocities span a disk due to the lattice regularization in the k_y-direction, Eqs. (2a) and (8). The parameter η is the fermion anomalous dimension [Eq. (5)]. For $\eta > 0$, there is a divergence of the x-velocities near the speed of light (band velocity $v_F = 1$). At $\eta = 0$ (noninteracting initial condition), large x velocities are suppressed by Pauli blocking (see text).

Window for collisionless dynamics.—The correlator in Eq. (5) with $\eta > 0$ arises due to generic short-ranged interactions in the initially decoupled chains. The postquench dynamics captured by Eq. (4) ignore interactions in the subsequent time evolution.

Beyond the density bump dynamics explored here, the main bulk effect of the global quench is to generate a finite density of particle-hole pairs, corresponding to a nonzero average energy per particle. If the interactions are not turned off at the time of the quench, then the system is expected to eventually thermalize to a temperature corresponding to the injected energy density [20].

We can estimate the collision rate $1/\tau_{\text{col}}$ responsible for thermalization in the postquench evolution. For the low-energy pi-flux Dirac fermions, a short-ranged lattice interaction carries units of energy $\times$ length$^2 \sim U_f a^2$, where U_f is the lattice interaction energy. The subscript "f" denotes the interaction strength after the quench, which can differ from the prequench strength $\equiv U_i$. The postquench Fermi golden rule collision rate should be of order $1/\tau_{\text{col}} \sim [(U_f a^2)/(b v_F^2)]^2 \varepsilon^3$, where ε is the characteristic energy per particle. The two factors of $b^{-1} v_F^{-2}$ arise from the density of states. For $k_F = 0$ (half filling), a crude estimate is $\varepsilon \sim b v_F/a \sim bJ$, so that

$$bJ\tau_{\text{col}} \sim (J/U_f)^2. \tag{9}$$

In the postquench evolution, time is measured in units of $1/bJ$ ($b = 1$ in Figs. 2 and 3). Equation (9) implies that the window of time over which collisionless dynamics can occur is set by the dimensionless ratio of U_f/J. At times $t \gg \tau_{\text{col}}$, we expect the ultimate density wave evolution to be governed by classical hydrodynamics [19].

Small U_f/J will induce a large collisionless window. By contrast, the anomalous dimension η responsible for the supersoliton dynamics in Fig. 2 is a function of the ratio U_i/J. Taking the latter to be too small will result in $\eta \ll 1$. For spin-1/2 Hubbard chains with repulsive interactions and $U_i/J \sim 1$, it is possible to get K close to $1/2$ ($\eta = 1/8$) for particle densities very close but not equal to half-filling [15,38]. In Ref. [37], we show, for example, that $\eta = 0.2$ still exhibits the supersoliton over the same time interval as Fig. 2.

A balance should be struck between minimizing collisions over a sufficiently long time window after the quench, and maximizing the correlations in the initial state. At the same time, in an optical lattice setup for ultracold fermions $U_f < U_i$, since lowering the tunneling barriers in the y direction to couple the 1D chains together will necessarily "unsqueeze" the atoms in that direction, decreasing the on-site interaction energy. A further reduction of U_f and (enhancement of τ_{col}) is possible if at the time of the quench the confinement is simultaneously reduced in the z direction, perpendicular to the plane of the 2D lattice.

We thank Kaden Hazzard and Randy Hulet for helpful discussions. We thank Stephen Bradshaw, Anthony Sciola, Jia-Liang Shen, and Shah Alam for helpful discussions on high-performance computing. This work was supported in part by the Data Analysis and Visualization Cyberinfrastructure funded by NSF under Grant No. OCI-0959097 and Rice University. M. S. F. acknowledges support from the U.S. Army Research Office (Grant No. W911NF-17-1-0259). This research was also supported by NSF CAREER Grant No. DMR-1552327, and by the Welch Foundation Grant No. C-1809. M. S. F. thanks the Aspen Center for Physics, which is supported by the NSF Grant No. PHY-1607611, for its hospitality while part of this work was performed.

[1] P. A. Lee, N. Nagaosa, and X.-G. Wen, Doping a Mott insulator: Physics of high-temperature superconductivity, Rev. Mod. Phys. **78**, 17 (2006).
[2] S. Sachdev, Exotic phases and quantum phase transitions: Model systems and experiments, arXiv:0901.4103.
[3] C. Nayak, S. H. Simon, A. Stern, M. Freedman, and S. D. Sarma, Non-Abelian anyons and topological quantum computation, Rev. Mod. Phys. **80**, 1083 (2008).
[4] R. L. Willett, L. N. Pfeiffer, and K. W. West, Measurement of filling factor 5/2 quasiparticle interference with observation of charge $e/4$ and $e/2$ period oscillations, Proc. Natl. Acad. Sci. U.S.A. **106**, 8853 (2009); D. T. McClure, W. Chang, C. M. Marcus, L. N. Pfeiffer, and K. W. West, Fabry-Perot Interferometry with Fractional Charges, Phys. Rev. Lett. **108**, 256804 (2012).
[5] N. R. Cooper, J. Dalibard, and I. B. Spielman, Topological bands for ultracold atoms, arXiv:1803.00249.
[6] G. Pagano, M. Mancini, G. Cappellini, P. Lombardi, F. Schäfer, H. Hu, X.-J. Liu, J. Catani, C. Sias, M. Inguscio, and L. Fallani, A one-dimensional liquid of fermions with tunable spin, Nat. Phys. **10**, 198 (2014).
[7] T. L. Yang, P. Grišins, Y. T. Chang, Z. H. Zhao, C. Y. Shih, T. Giamarchi, and R. G. Hulet, Measurement of the Dynamical Structure Factor of a 1D Interacting Fermi Gas, Phys. Rev. Lett. **121**, 103001 (2018).
[8] D. Greif, G. Jotzu, M. Messer, R. Desbuquois, and T. Esslinger, Formation and Dynamics of Antiferromagnetic Correlations in Tunable Optical Lattices, Phys. Rev. Lett. **115**, 260401 (2015).
[9] M. Aidelsberger, M. Atala, M. Lohse, J. T. Berreiro, B. Paredes, and I. Bloch, Realization of the Hofstadter Hamiltonian with Ultracold Atoms in Optical Lattices, Phys. Rev. Lett. **111**, 185301 (2013).
[10] H. Miyake, G. A. Siviloglou, C. J. Kennedy, W. C. Burton, and W. Ketterle, Realizing the Harper Hamiltonian with Laser-Assisted Tunneling in Optical Lattices, Phys. Rev. Lett. **111**, 185302 (2013).
[11] C. J. Kennedy, W. C. Burton, W. C. Chung, and W. Ketterle, Observation of Bose-Einstein condensation in a strong synthetic magnetic field, Nat. Phys. **11**, 859 (2015).
[12] J. Cardy, *Scaling and Renormalization in Statistical Physics* (Cambridge University Press, Cambridge, England, 1996).

[13] S. Sachdev, *Quantum Phase Transitions*, 2nd ed. (Cambridge University Press, Cambridge, England, 2007).
[14] A. O. Gogolin, A. A. Nersesyan, and A. M. Tsvelik, *Bosonization and Strongly Correlated Systems* (Cambridge University Press, Cambridge, England, 1998).
[15] T. Giamarchi, *Quantum Physics in One Dimension* (Clarendon Press, Oxford, England, 2003).
[16] M. A. Cazalilla, Effect of Suddenly Turning on Interactions in the Luttinger Model, Phys. Rev. Lett. **97**, 156403 (2006).
[17] M. Moeckel and S. Kehrein, Interaction Quench in the Hubbard Model, Phys. Rev. Lett. **100**, 175702 (2008).
[18] M. Eckstein, M. Kollar, and P. Werner, Thermalization after an Interaction Quench in the Hubbard Model, Phys. Rev. Lett. **103**, 056403 (2009).
[19] U. Schneider, L. Hackermüller, J. P. Ronzheimer, S. Will, S. Braun, T. Best, I. Bloch, E. Demler, S. Mandt, D. Rasch, and A. Rosch, Fermionic transport and out-of-equilibrium dynamics in a homogeneous Hubbard model with ultracold atoms, Nat. Phys. **8**, 213 (2012).
[20] M. Tavora and A. Mitra, Quench dynamics of one-dimensional bosons in a commensurate periodic potential: A quantum kinetic equation approach, Phys. Rev. B **88**, 115144 (2013).
[21] S. Ngo Dinh, D. A. Bagrets, and A. D. Mirlin, Interaction quench in nonequilibrium Luttinger liquids, Phys. Rev. B **88**, 245405 (2013).
[22] A. J. A. James and R. M. Konik, Quantum quenches in two spatial dimensions using chain array matrix product states, Phys. Rev. B **92**, 161111(R) (2015).
[23] I. G. White, R. G. Hulet, and K. R. A. Hazzard, Correlations generated from high-temperature states: Nonequilibrium dynamics in the Fermi-Hubbard model, arXiv:1612.05671.
[24] X. Yin and L. Radzihovsky, Quench dynamics of the spin-imbalanced Fermi-Hubbard model in one dimension, Phys. Rev. A **94**, 063637 (2016).
[25] For a recent review, see A. Mitra, Quantum Quench Dynamics, Annu. Rev. Condens. Matter Phys. **9**, 245 (2018).
[26] E. Bettelheim, A. G. Abanov, and P. Wiegmann, Orthogonality Catastrophe and Shock Waves in a Nonequilibrium Fermi Gas, Phys. Rev. Lett. **97**, 246402 (2006).
[27] M. S. Foster, E. A. Yuzbashyan, and B. L. Altshuler, Quantum Quench in One Dimension: Coherent Inhomogeneity Amplification and "Supersolitons," Phys. Rev. Lett. **105**, 135701 (2010).
[28] M. S. Foster, T. C. Berkelbach, D. R. Reichman, and E. A. Yuzbashyan, Quantum quench spectroscopy of a Luttinger liquid: Ultrarelativistic density wave dynamics due to fractionalization in an *XXZ* chain, Phys. Rev. B **84**, 085146 (2011).
[29] J. Mossel1 and J.-S. Caux, Relaxation dynamics in the gapped XXZ spin-1/2 chain, New J. Phys. **12**, 055028 (2010).
[30] J. Lancaster and A. Mitra, Quantum quenches in an XXZ spin chain from a spatially inhomogeneous initial state, Phys. Rev. E **81**, 061134 (2010).
[31] J. Lancaster, E. Gull, and A. Mitra, Quenched dynamics in interacting one-dimensional systems: Appearance of current-carrying steady states from initial domain wall density profiles, Phys. Rev. B **82**, 235124 (2010).
[32] C. Neuenhahn, A. Polkovnikov, and F. Marquardt, Localized Phase Structures Growing Out of Quantum Fluctuations in a Quench of Tunnel-coupled Atomic Condensates, Phys. Rev. Lett. **109**, 085304 (2012).
[33] J. L. Lancaster, Nonequilibrium current-carrying steady states in the anisotropic XY spin chain, Phys. Rev. E **93**, 052136 (2016).
[34] B. Bertini, M. Collura, J. De Nardis, and M. Fagotti, Transport in Out-of-Equilibrium XXZ Chains: Exact Profiles of Charges and Currents, Phys. Rev. Lett. **117**, 207201 (2016).
[35] B. Doyon, J. Dubail, R. Konik, and T. Yoshimura, Large-Scale Description of Interacting One-Dimensional Bose Gases: Generalized Hydrodynamics Supersedes Conventional Hydrodynamics, Phys. Rev. Lett. **119**, 195301 (2017).
[36] M. Kormos, Inhomogeneous quenches in the transverse field Ising chain: Scaling and front dynamics, SciPost Phys. **3**, 020 (2017).
[37] See Supplemental Material at http://link.aps.org/supplemental/10.1103/PhysRevLett.122.065302 for the derivation of the theory in Eq. (2a) from Eq. (1), the precise specification of the integrals evaluated to obtain the results in Figs. 2, 3, and 4, error analysis of these, the effects of short-distance regularization on the dynamics, and for comparison to the single-particle wave packet dynamics in the pi-flux band structure.
[38] H. J. Schulz, Correlation Exponents and the Metal-Insulator Transition in the One-Dimensional Hubbard Model, Phys. Rev. Lett. **64**, 2831 (1990).